magnetism

MDPI

Article

Kinetics of Domain Structure in Co/Pt/Co Ultrathin Films with Ferromagnetic Interlayer Exchange Interaction: Dependence on Interlayer Thickness

Ivan Shashkov, Yuri Kabanov, Oleg Tikhomirov and Vladimir Gornakov *

Institute of Solid State Physics RAS, 142432 Chernogolovka, Russia; shav@issp.ac.ru (I.S.); kayur@issp.ac.ru (Y.K.); tikhomir@issp.ac.ru (O.T.)
* Correspondence: gornakov@issp.ac.ru

Abstract: We studied the in-field evolution of the domain structure in ultrathin Co(0.6 nm)/Pt(t)/Co(0.6) nm trilayers with perpendicular magnetic anisotropy for 5 nm < t < 6 nm using polar Kerr microscopy. The critical interlayer thickness t_{cr} = 5.3 nm was found to separate two principal patterns of domain behavior including interlayer correlations and motility of the domain walls. It is shown that magnetization in both Co layers is coupled with strong ferromagnetic interaction for small Pt thickness ($t < t_{cr}$), while this coupling is weak for thicker ($t > t_{cr}$) Pt layers. Nonlinear dependence of the wall displacement on the field value is observed. The established final position of domain walls after relaxation depends on the Pt layer thickness. It is determined by balance of the interlayer exchange and energy gain due to the field. The mechanism of wall stabilization is considered in the case of independent wall motion. In the region with weak coupling, dependence of the interlayer interaction energy on Pt thickness was measured.

Keywords: domain wall dynamics; magnetic multilayers; interlayer exchange interaction

check for updates

Citation: Shashkov, I.; Kabanov, Y.; Tikhomirov, O.; Gornakov, V. Kinetics of Domain Structure in Co/Pt/Co Ultrathin Films with Ferromagnetic Interlayer Exchange Interaction: Dependence on Interlayer Thickness. *Magnetism* **2022**, *2*, 186–194. https://doi.org/10.3390/magnetism2020014

Academic Editor: Zhidong Zhang

Received: 1 June 2022
Accepted: 15 June 2022
Published: 16 June 2022

1. Introduction

Magnetic thin film structures with perpendicular magnetic anisotropy (PMA) possess unique physical properties [1–3]. They can be used as model materials to investigate the formation and evolution of specific domain structures [4–8], thermoactivated domain wall creep [9], magnetoresistance [10], anomalous Hall effect [10,11], and spin-wave dynamics [12]. The list of possible applications includes high-density magnetic memory devices [13,14], magnetic sensors for medicine [15], and superfast elements for spintronics [16]. Switching of magnetization in such materials involves nucleation of new domains and motion of domain walls (DWs) [4,8,17–21]. These processes are well examined in the case of continuous ultrathin ferromagnetic (FM) Co films with PMA [17–19,22]. Meanwhile, they can be quite different in the case of a superlattice where PMA layers are separated by nonmagnetic (NM) layers [23–25]. Depending on the number and thickness of both FM and NM layers, different magnetic phases can be observed, including stable interlayer frustration at the domain walls. Switching of such complicated objects in multiple layers can be highly inhomogeneous, and its mechanism is difficult to understand.

More distinct are similar phenomena in trilayers where two FM layers are still coupled across the NM layer by exchange or magnetostatic interaction J [1,3–9,26,27]. Typical for exchange coupling is its dependence on the thickness of the NM layer. It was shown theoretically [28,29] and experimentally [26,30,31] that this dependence is oscillatory. Studying magnetoresistance and the Kerr effect in a wedge-shaped trilayer Co/Au(111)/Co, the authors of [31] showed that the mutual orientation of magnetization in FM layers changed from parallel to antiparallel and back when the Au thickness was varied monotonically; that is, interlayer exchange evolved from ferromagnetic to antiferromagnetic and vice versa. However, the mechanism of the magnetization reversal was not revealed. Nucleation and motion of the domain walls were observed for both exchange ([4–9] Co/Pt/Co) and magnetostatic ([27] CoPt/NiO/CoPt) interactions between FM layers. Dependence of the DW velocity on the applied field was investigated both theoretically and experimentally in separate FM layers of different thickness and in a coupled trilayer system [5–9]. It was shown that despite the DWs having different mobility in each separate layer, they proceeded together with the same speed in the case of ferromagnetic coupling between the FM layers. Thickness-dependent coupling parameter J can be determined by measuring the minor hysteresis loops using the magneto-optic Kerr effect [8] or using ferromagnetic resonance studies [26]. Experiments with similar Co/Pt/Co trilayers where the NM Pt layer was wedge-shaped revealed a transition of the domain nucleation pattern and domain wall motion depending on the Pt thickness and, hence, on the strength of interlayer coupling [4,8]. When the thickness of the Pt layer was above some critical value, nucleation of new domains and motion of domain walls in both FM layers were independent and uncorrelated, while the processes were synchronous in the case of thinner Pt interlayers. These features should be determined by kinetics and relaxation of the domain structure depending on the interlayer interaction. Detailed analysis of this problem is the purpose of the present paper.

2. Experiment

The sample used in our experiments was a Pt(10 nm)/Co(0.6 nm)/Pt(t)/Co(0.6 nm)/Pt(3 nm) structure synthesized by magnetron sputtering on a 5 × 6 mm oxidized silicon substrate at room temperature. Thickness of the Pt layer increased uniformly from 5 to 6 nm (Figure 1). The hysteresis loops were obtained by measuring the intensity of the Kerr effect from local (0.3 × 0.3) mm areas of the sample. Domain structure and DW motion were studied by magneto-optic (MO) microscopy based on the Kerr effect. To improve the magneto-optic contrast, we registered preliminary images of the saturated sample in a strong positive and negative magnetic field. The average of these two magneto-optic pictures was subtracted from every experimental image of the transient domain structure.

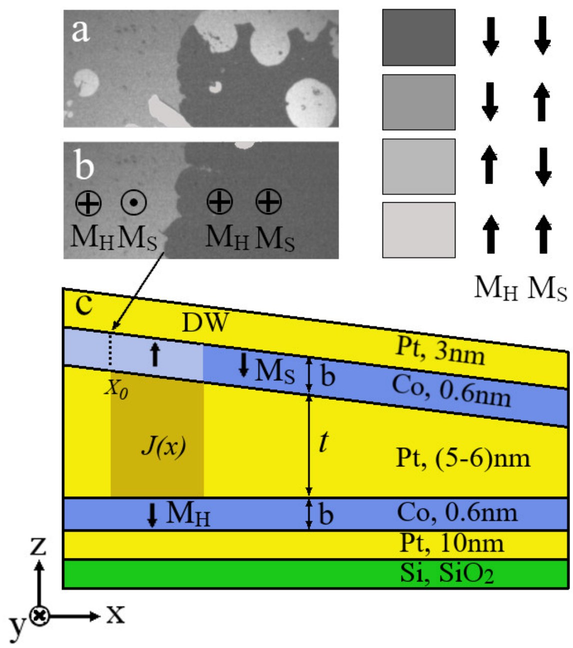

Figure 1. Magneto-optic images of the FM/NM/FM trilayer (**a**) after application of series of magnetic field pulses $H = \pm 100$ Oe, and (**b**) after further formation of a single domain wall near $x = x_0$ with an AC magnetic field $H = H_c$; (**c**) general view of the sample with magnetization in FM layers. Magnetizations M_S and M_H correspond to soft and hard layers, as determined below.

3. Results and Discussion

Contrary to [5–8] where FM layers in Co/Pt/Co had different thickness, we performed a direct experimental investigation with equal thickness of FM layers but with a spatially varying NM layer. Magnetization of both Co layers was the same. Similar to [4], kinetics of the magnetization reversal was different at opposite sides of the sample. Application of a number of field pulses (4 ms, ±100 Oe) resulted in the formation of a complicated domain structure. Four principal configurations of mutual orientation of magnetization in both FM layers could be extracted from magneto-optic Kerr images (Figure 1a). Further magnetic treatment using a 10 Hz AC magnetic field with amplitude close to coercivity allowed obtaining a solitary domain wall at the position x_0 where the antiferromagnetic interaction between FM layers was replaced with a ferromagnetic one (Figure 1b). Examination of the Kerr intensity along the wedge confirmed that the magnetization in FM layers was parallel (that is, the interlayer coupling was ferromagnetic) everywhere for $x > x_0$. In the field H = +800 Oe normal to the surface, both FM layers were saturated (phase I). Elimination of this field and application of a field with opposite sign caused nucleation of new domains and motion of domain walls.

When the Pt layer was thin, the switching proceeded via coherent nucleation of new domains (phase III) in both FM layers (Figure 2a). DW motion was also coupled in both layers. Figure 2b shows the profile of the MO signal intensity I across the domain wall. Intensities in domain states I and III corresponded to complete saturation values; hence, positions of the domain wall in both layers coincided exactly. The local MO hysteresis loop was strictly rectangular (Figure 2c), confirming coupled motion of the walls in both layers. This picture was observed in all areas where t < 5.4 nm.

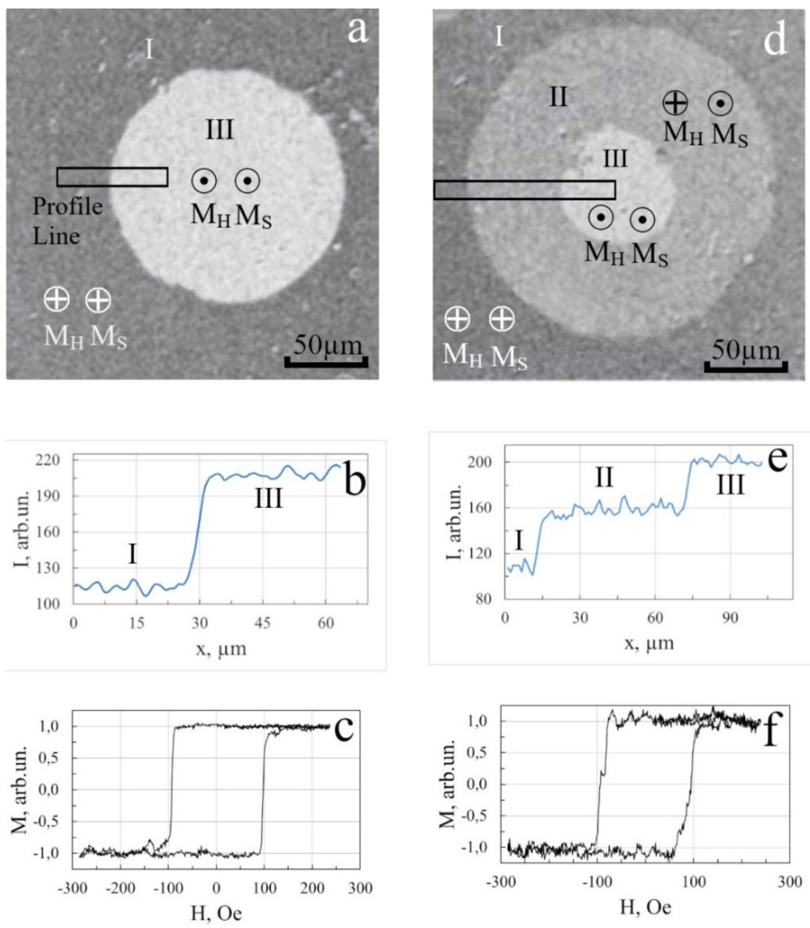

Figure 2. (**a**,**d**) Magneto-optic images of the domain structure; (**b**,**e**) profiles of the Kerr intensity across the domain wall; (**c**,**f**) magneto-optic hysteresis loops for $t < t_{cr}$ (**a**–**c**) and $t > t_{cr}$ (**d**–**f**).

When t was higher than this critical value, both the DW image and the MO profile were different. The new domains arose at different fields in the top FM layer and the lower one, and their domain walls moved independently. As a rule, the process began in one Co layer (magnetically soft layer with magnetization M_S), and, when it was reversed completely (phase II), nucleation and DW motion began in the second layer (magnetically hard layer with magnetization M_H) (Figure 2d). To distinguish which layer was switched first, we analyzed the corresponding MO profile (Figure 2e). The Kerr intensity was obviously weaker for the bottom FM layer.

The intensity of the total MO signal in the three phases described above was I^{I}, I^{II}, and I^{III}.

$$\begin{aligned} I^{I} &= I_{1\uparrow} + I_{2\uparrow}, \\ I^{II} &= I_{1\uparrow} + I_{2\downarrow}, \\ I^{III} &= I_{1\downarrow} + I_{2\downarrow}. \end{aligned} \tag{1}$$

The separate intensity of each layer I_1 and I_2 magnetized up or down was determined by the Malus law.

$$\begin{aligned} I_{1\uparrow} &= I_0\,\mathrm{Cos}^2(\beta + \varphi_1) = I_0\,[(\mathrm{Cos}(\beta)\,\mathrm{Cos}(\varphi_1) - \mathrm{Sin}(\beta)\,\mathrm{Sin}(\varphi_1)]^2, \\ I_{1\downarrow} &= I_0\,\mathrm{Cos}^2(\beta - \varphi_1) = I_0\,[(\mathrm{Cos}(\beta)\,\mathrm{Cos}(\varphi_1) + \mathrm{Sin}(\beta)\,\mathrm{Sin}(\varphi_1)]^2, \\ I_{2\uparrow} &= I_0\,\mathrm{Cos}^2(\beta + \varphi_2) = I_0\,[(\mathrm{Cos}(\beta)\,\mathrm{Cos}(\varphi_2) - \mathrm{Sin}(\beta)\,\mathrm{Sin}(\varphi_2)]^2, \\ I_{2\downarrow} &= I_0\,\mathrm{Cos}^2(\beta - \varphi_2) = I_0\,[(\mathrm{Cos}(\beta)\,\mathrm{Cos}(\varphi_2) + \mathrm{Sin}(\beta)\,\mathrm{Sin}(\varphi_2)]^2, \end{aligned} \tag{2}$$

where I_0 is the intensity of incident light polarized linearly, β is the rotation of the polarization plane when two polarizers are slightly uncrossed, and φ_1 and φ_2 are angles of rotation induced by magnetization M_1 and M_2 of two FM layers.

The intensity provided by each layer could be estimated from the MO profile across DW (Figure 2e).

$$\begin{aligned} I^{II} - I^{I} &= I_0\,\mathrm{Sin}(2\beta)\,\mathrm{Sin}(2\varphi_2) \approx D\,2\varphi_2, \\ I^{III} - I^{II} &= I_0\,\mathrm{Sin}(2\beta)\,\mathrm{Sin}(2\varphi_1) \approx D\,2\varphi_1, \end{aligned} \tag{3}$$

where $D = I_0\sin(2\beta)$ is a constant value, and $\sin(2\varphi_{1,2})$ at small φ is approximately $2\varphi_{1,2}$. Therefore, the difference in MO intensity across domain walls (Figure 2d) was determined by the rotation angle in a corresponding layer. The measured values of $I^{II} - I^{I}$ and $I^{III} - I^{II}$ were 50 and 42, respectively. This means that both nucleation of new domains and DW motion started in the upper Co layer where the MO signal was strongest.

The difference in coercivity of lower (hard) and upper (soft) Co layers allowed us to directly observe incoherent nucleation and separated domain walls, DW_S and DW_H, as well as motion in these soft and hard layers, respectively. The local MO hysteresis loop in this area of the sample is not rectangular (Figure 2f) exhibiting consecutive magnetization reversal. The typical separate steps often observed in magnetic multilayers [1,9,10,31] were not well resolved as the difference in coercivity was rather small. The measured values of the start field in both layers (Figure 2d) were H_{c1} = 24 Oe and H_{c2} = 30 Oe. The measured intensity difference ($I^{III} - I^{I}$) was the same for both thin (Figure 2b) and thick (Figure 2e) Pt layers as the total thickness of the FM layer remained constant.

While the bottom FM layer showed the same picture of magnetization reversal for every position along the sample, switching of the top layer depended on the interlayer Pt thickness when $t > t_{cr}$. Figure 3a shows the consecutive displacement of the DW toward the thinner side of the Pt wedge when a sequence of H = 50 Oe, τ = 4 ms magnetic field pulses was applied. After each single pulse, the domain wall shifted to a new position passing the distance $\Delta x_i = x_{i+1} - x_i$, where i is the number of pulses. Total displacement of the wall is shown in Figure 3b. Figure 3a shows that, when the wall approached the position where $t = t_{cr}$, its displacement after each pulse became smaller before finally (here, after the 25th pulse) reaching zero, such that the wall reached its equilibrium position for a given amplitude of the field pulse (Figure 3b).

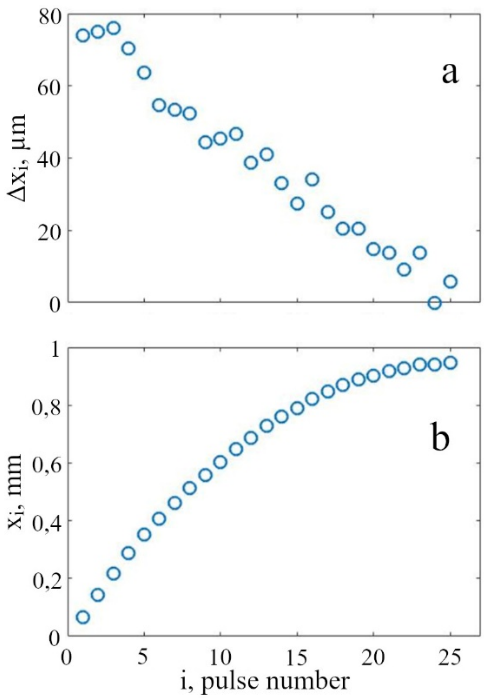

Figure 3. Displacement of the domain wall (**a**) after every *i*-th pulse of the field; (**b**) total displacement after series of *i* pulses, H = 50 Oe, τ = 4 ms.

Figure 4 shows the dependence of the DW position on the amplitude of the field after some transient series of pulses (5–9). Duration τ = 4 ms was chosen such that the upper DW could move ahead of the bottom one as shown in Figure 4 (inserts I and II). The distance between the two walls was much larger than the wall thickness; thus, their motion was likely independent. The two wall displacements x_1 and x_2 became comparable only near t_{cr} (insert III in Figure 4). Dependence $x_i(H)$ was obviously nonlinear, tending to stop in the vicinity of the value corresponding to $t = t_{cr}$. When the upper DW reached the part of the sample where $t \leq t_{cr}$, it did not move despite a further increase in the field amplitude until the lower wall joined it. Subsequently, both walls moved together as a single object.

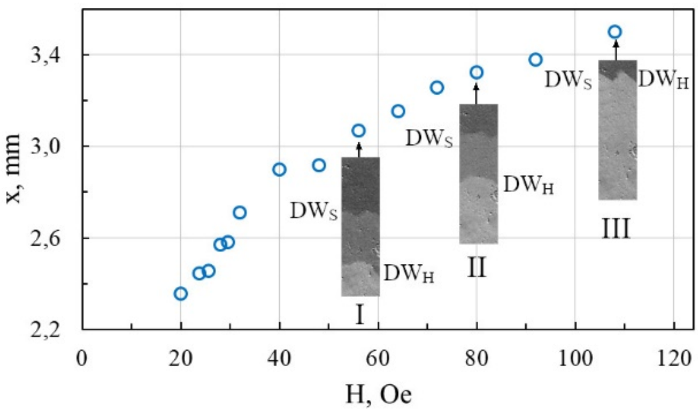

Figure 4. Equilibrium positions (as shown in Figure 3b) of the domain wall in the top ferromagnetic layer after application of a series of magnetic field pulses as a function of their amplitude. Inserts show typical magneto-optic images of walls in both top and bottom layers.

The observed monotonic decrease in the DW displacement with every field pulse when it moved from the thicker interlayer side to the thinner one assumed the presence of an additional effective field $H_J(x)$. This additional field was antiparallel to the driving one, and its value increased with a decrease in interlayer thickness t. The free energy necessary to move the wall in the x-direction can be written as

$$\Delta W(x) = 2(H - H_{c1} - H_J(x))\, M\, Y\, b\, x, \quad (4)$$

where b is the thickness of the FM layer, Y is the length of DW along the y-axis, and H and H_{c1} are the driving field and coercivity of the upper layer, respectively. DW stopped at some new position x (Figure 4) when it reached the new equilibrium state $\Delta W(x) = 0$. That is,

$$2(H - H_{c1} - H_J(x))\, M\, Y\, b\, x = 0, \quad (5)$$

or

$$H_J(x) = (H - H_c). \quad (6)$$

By subtracting coercivity from the driving field and taking into account the relation in Equation (6), one can determine dependence $H_J(x)$. It is shown in Figure 5a (circles). The initial left point x_0 where the interlayer exchange field changed its sign ($J = 0$) was determined separately by moving the upper DW with an AC magnetic field around this point with the same field amplitude $H \approx H_c$.

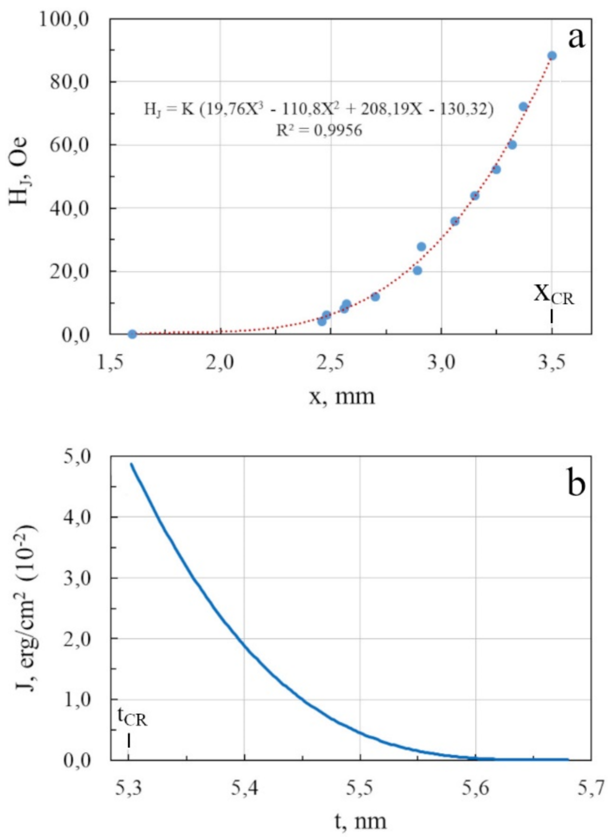

Figure 5. (**a**) Measured dependence of the effective field of interlayer coupling on position in the wedge (circles) and its polynomial approximation (solid line); (**b**) extracted dependence of interlayer exchange coupling on thickness of the nonmagnetic Pt layer.

Equation (5) can be written as

$$2(H - H_c)\, M\, Y\, b\, x = 2H_J(x)\, M\, Y\, b\, x. \quad (7)$$

Effective field $H_J(x)$ preventing DW motion was caused by an interlayer exchange interaction $J(x)$ between FM Co layers, taking into account the enhancement of energy when the moving DW passed the surface S

$$\Delta W(x) = 2(H - H_c)\, M\, Y\, b\, x - \int J(x)\, dS = 0, \tag{8}$$

$$2(H - H_c)\, M\, Y\, b\, x = \int J(x)\, dS = Y \int J(x)\, dx, \tag{9}$$

where $S = Yx$ is the surface swept by the wall during its motion.

Equations (7) and (9) result to

$$H_J(x) = (2M\, b\, x)^{-1} \int J(x) dx. \tag{10}$$

Separating the variables yields

$$x\, H_J(x) = (2\, M\, b)^{-1} \int J(x) dx. \tag{11}$$

Finally, taking the derivative, one gets dependence $J(x)$,

$$J(x) = 2\, M\, b\, (H_J(x) + x\, dH_J(x)/dx). \tag{12}$$

The measured dependence $H_J(x)$ fits a third-degree polynomial (shown by the line in Figure 5a),

$$H_J = K\, (19.76\, X^3 - 110.8\, X^2 + 208.19\, X - 130.32), \tag{13}$$

where $K = 1$ Oe and dimensionless variable $X = x/1$ mm. Equations (12) and (13) allow deducing dependence $J(x)$ from the experimental data. The interlayer thickness varies linearly with x with a factor of $C = -\Delta t/\Delta x = -0.2$ nm/mm, $t = t_0 + Cx$, where Δt is the maximal change in interlayer thickness in the interval under study (1 nm), and t_0 is the maximal interlayer thickness (6 nm); hence, dependence $J(x)$ can be easily recalculated to $J(t)$. The final dependence $J(t)$ is shown in Figure 5b.

Thus, we obtained the detailed dependence $J(t)$ in the FM/NM/FM wedge heterostructure in the area with ferromagnetic interlayer interaction, $J(t) > 0$. It is shown that the energy density increased for thinner Pt layers. Furthermore, this rise was steeper when thickness approached t_{cr}. The effective magnetic field $H(t)$ due to exchange interaction between layers also increased with the decrease in t (i.e., increase in x). This is the reason for the asymmetric domain nucleation and domain wall motion observed in [4]. According to Equation (6), the wall moves when $H - H_j > H_c$. Otherwise, the walls stop, in agreement with Figure 4. However, the quick rise in $J(t)$ and $H_j(t)$ when the wall moved toward a thinner Pt area resulted in a stronger counteraction of H_j. Hence, one needs to increasingly enhance driving field H while the wall travels progressively smaller distance. Finally, the individual motion of the wall becomes suppressed when its displacement exceeds x_{cr}. Application of an even stronger H leads to joined motion of the top and bottom domain walls, as observed in [4].

The origin of the observed distinction in the switching scenarios at $t > t_{cr}$ and $t < t_{cr}$ is the relationship of the exchange energy $J(t)$ and energy $W_{C2} = 2MH_{C2}b$ necessary to overcome coercivity in the bottom FM layer. $J(t) < W_{c2}$ when $t > t_{cr}$ (or $x < x_{cr}$). In this case, the upper domain wall can move separately as the interlayer exchange cannot overcome pinning of the wall in the bottom layer. If $J(t) > W_{c2}$ ($t < t_{cr}$, $x > x_{cr}$), the interlayer exchange is capable of pulling the bottom wall, and both walls travel together.

4. Conclusions

We performed measurements of the field-driven domain wall displacement along the FM/NM/FM wedge heterostructure using the magneto-optic Kerr effect. This procedure allowed us to extract the dependence of the effective field on the interlayer thickness $H_j(t)$. Hence, we obtained the detailed dependence $J(t)$ in the area with ferromagnetic interlayer interaction. It was shown that $H_j(t)$ and $J(t)$ increased significantly with the decrease in Pt thickness. The obtained values of 0 erg/cm^2 < J < 5·10^{-2} erg/cm^2 with ~5.6 nm > t > t_{cr} = 5.3 nm are in good agreement with the results reported by other authors [8,31]. We studied the transition between the two switching scenarios of the FM/NM/FM wedge for $t < t_{cr}$ and $t > t_{cr}$ observed in [4,8]. It is shown that the nonlinear growth of interlayer exchange requires progressively increasing the driving field to push the domain wall toward the thin platinum layer side. The separated motion of the wall in the top FM layer becomes suppressed, and, for a higher field, the walls in both layers move together, as observed in [4]. Distinction between the two regimes of the wall motion is determined by the relationship between the interlayer exchange field and pinning in the bottom layer, i.e., when $J(t)$ becomes equal to or greater than energy W_{C2}, as determined by the coercivity H_{C2} of the bottom layer.

Author Contributions: Conceptualization, Y.K. and V.G.; methodology, V.G.; formal analysis, V.G.; investigation, I.S. and Y.K.; data curation, I.S. and Y.K.; writing—original draft preparation, V.G. and O.T.; writing—review and editing, V.G. and O.T.; visualization, O.T.; supervision, V.G.; project administration, V.G. All authors have read and agreed to the published version of the manuscript.

Funding: This research was performed in the framework of the State Task program of the Institute of Solid State Physics, Russian Academy of Science.

Data Availability Statement: The data are available from the authors on reasonable demand.

Conflicts of Interest: The authors declare no conflict of interest.

References

1. Heinrich, B.; Cochran, J.F. Ultrathin metallic magnetic films: Magnetic anisotropies and exchange interactions. *Adv. Phys.* **1993**, *42*, 523–639. [CrossRef]
2. Johnson, M.T.; Jungblut, R.; Kelly, P.J.; den Breeder, F.J.A. Perpendicular magnetic anisotropy of multilayers: Recent insights. *J. Magn. Magn. Mat.* **1995**, *148*, 118–124. [CrossRef]
3. Omelchenko, P.; Montoya, E.; Girt, E.; Heinrich, B. Interlayer Exchange Coupling, Spin Pumping and Spin Transport in Metallic Magnetic Single and Bilayer Structures. *J. Exp. Theor. Phys.* **2020**, *131*, 113–129. [CrossRef]
4. Shull, R.D.; Iunin, Y.L.; Kabanov, Y.P.; Nikitenko, V.I.; Skryabina, O.V.; Chien, C.L. Influence of Pt spacer thickness on the domain nucleation in ultrathin Co/Pt/Co trilayers. *J. Appl. Phys.* **2013**, *113*, 17C101. [CrossRef]
5. Metaxas, P.J.; Stamps, R.L.; Jamet, J.-P.; Ferre, J.; Baltz, V.; Rodmacq, B.; Politi, P. Dynamic Binding of Driven Interfaces in Coupled Ultrathin Ferromagnetic Layers. *Phys. Rev. Lett.* **2010**, *104*, 237206. [CrossRef]
6. Politi, P.; Metaxas, P.J.; Jamet, J.-P.; Stamps, R.L.; Ferre, J. Model of bound interface dynamics for coupled magnetic domain walls. *Phys. Rev. B* **2011**, *84*, 054431. [CrossRef]
7. Metaxas, P.J.; Stamps, R.L.; Jamet, J.-P.; Ferre, J.; Baltz, V.; Rodmacq, B. Expansion and relaxation of magnetic mirror domains in a Pt/Co/Pt/Co/Pt multilayer with antiferromagnetic interlayer coupling. *J. Phys. Condens. Matter* **2012**, *24*, 024212. [CrossRef] [PubMed]
8. Matczak, M.; Schäfer, R.; Urbaniak, M.; Kuświk, P.; Szymański, B.; Schmidt, M.; Aleksiejew, J.; Stobiecki, F. Influence of domain structure induced coupling on magnetization reversal of Co/Pt/Co film with perpendicular anisotropy. *J. Magn. Magn. Mat.* **2017**, *422*, 465–469. [CrossRef]
9. Metaxas, P.J.; Jamet, J.P.; Ferre, J.; Rodmacq, B.; Dieny, B.; Stamps, R.L. Magnetic domain wall creep in the presence of an effective interlayer coupling field. *J. Magn. Magn. Mat.* **2008**, *320*, 2571–2575. [CrossRef]
10. Zhang, F.; Liu, Z.; Wen, F.; Liu, Q.; Li, X.; Ming, X. Magnetoresistance and Anomalous Hall Effect with Pt Spacer Thickness in the Spin-Valve Co/Pt/[Co/Pt]$_2$ Multilayers. *J. Supercond. Nov. Magn.* **2017**, *30*, 533–538. [CrossRef]
11. Liua, Q.; Jiang, S.; Teng, J. Interfacial chemical structure-modulated anomalous Hall effect in perpendicular Co/Pt multilayers. *J. Appl. Surf. Sci.* **2018**, *433*, 556–559. [CrossRef]
12. Szulc, K.; Mendisch, S.; Mruczkiewicz, M.; Casoli, F.; Becherer, M.; Gubbiotti, G. Nonreciprocal spin-wave dynamics in Pt/Co/W/Co/Pt multilayers. *Phys. Rev. B* **2021**, *103*, 134404. [CrossRef]
13. Moritz, J.; Rodmacq, B.; Auffret, S.; Dieny, B. Extraordinary Hall effect in thin magnetic films and its potential for sensors, memories and magnetic logic applications. *J. Phys. D Appl. Phys.* **2008**, *41*, 135001. [CrossRef]
14. Dieny, B.; Chshiev, M. Perpendicular magnetic anisotropy at transition metal/oxide interfaces and applications. *Rev. Mod. Phys.* **2017**, *89*, 025008. [CrossRef]

15. Katagiri, M.; Cuya Huaman, J.L.; Matsumoto, T.; Suzuki, K.; Miyamura, H.; Balachandran, J. Magneto-Plasmonic Co@Pt@Au Nanocrystals for Biosensing and Therapeutics. *ACS Appl. Nano Mater.* **2020**, *3*, 418–427. [CrossRef]
16. Wilson, R.B.; Yang, Y.; Gorchon, J.; Lambert, C.-H.; Salahuddin, S.; Bokor, J. Electric current induced ultrafast demagnetization. *Phys. Rev. B* **2017**, *96*, 045105. [CrossRef]
17. Krusin-Elbaum, L.; Shibauchi, T.; Argyle, B.; Gignac, L.; Weller, D. Stable ultrahigh-density magneto-optical recordings using introduced linear defects. *Nature* **2001**, *410*, 444–446. [CrossRef] [PubMed]
18. Kabanov, Y.P.; Iunin, Y.L.; Nikitenko, V.I.; Shapiro, A.J.; Shull, R.D.; Zhu, L.Y.; Chien, C.L. In-plane field effects on the dynamics of domain walls in ultrathin Co films with perpendicular anisotropy. *IEEE Trans. Magn.* **2010**, *46*, 2220–2223. [CrossRef]
19. Jué, E.; Thiaville, A.; Pizzini, S.; Miltat, J.; Sampaio, J.; Buda-Prejbeanu, L.D.; Rohart, S.; Vogel, J.; Bonfim, M.; Boulle, O.; et al. Domain wall dynamics in ultrathin Pt/Co/AlOx microstrips under large combined magnetic fields. *Phys. Rev. B* **2016**, *93*, 014403. [CrossRef]
20. Morgunov, R.B.; Yurov, A.V.; Yurov, V.A.; Talantsev, A.D.; Bezverhnii, A.I.; Koplak, O.V. Oscillatory dynamics of the magnetic moment of a Pt/Co/Ir/Co/Pt synthetic antiferromagnet. *Phys. Rev. B* **2019**, *100*, 144407. [CrossRef]
21. Morgunov, R.B.; Bezverkhnii, A.I.; Hehn, M.; Bello, J.L.; Fache, T.; Mangin, S. Dzyaloshinskii-Moriya interaction probed by magnetization reversal in bilayer Pt/Co/Ir/Co/Pt synthetic ferrimagnets. *Phys. Rev. B* **2021**, *104*, 134424. [CrossRef]
22. Mazalski, P.; Anastaziak, B.; Kuświk, P.; Kurant, Z.; Sveklo, I.; Maziewski, A. Demagnetization of an ultrathin Co/NiO bilayer with creation of submicrometer domains controlled by temperature-induced changes of magnetic anisotropy. *J. Magn. Magn. Mat.* **2020**, *508*, 166871. [CrossRef]
23. Hellwig, O.; Berger, A.; Fullerton, E.E. Magnetic reversal and domain structure in perpendicular AF-coupled films. *J. Magn. Magn. Mat.* **2005**, *290–291*, 1–7. [CrossRef]
24. Hellwig, O.; Berger, A.; Kortright, J.B.; Fullerton, E.E. Domain structure and magnetization reversal of antiferromagnetically coupled perpendicular anisotropy films. *J. Magn. Magn. Mat.* **2007**, *319*, 13–55. [CrossRef]
25. Kiselev, N.S.; Bran, C.; Wolff, U.; Schultz, L.; Bogdanov, A.N.; Hellwig, O.; Neu, V.; Rößler, U.K. Metamagnetic domains in antiferromagnetically coupled multilayers with perpendicular anisotropy. *Phys. Rev. B* **2010**, *81*, 054409. [CrossRef]
26. Omelchenko, P.; Heinrich, B.; Girt, E. Measurements of interlayer exchange coupling of Pt in PyjPtjPy system. *Appl. Phys. Lett.* **2018**, *113*, 142401. [CrossRef]
27. Baruth, A.; Yuan, L.; Burton, J.D.; Janicka, K.; Tsymbal, E.Y.; Liou, S.H.; Adenwalla, S. Domain overlap in antiferromagnetically coupled multilayers. *Appl. Phys. Lett.* **2006**, *89*, 202505. [CrossRef]
28. Bruno, P.; Chappert, C. Ruderman-Kittel theory of oscillatory interlayer exchange coupling. *Phys. Rev. B* **1992**, *46*, 261. [CrossRef]
29. Stiles, M.D. Exchange coupling in magnetic heterostructures. *Phys. Rev. B* **1993**, *48*, 7238–7258. [CrossRef]
30. Parkin, S.S.P. Systematic variation of the strength and oscillation period of indirect magnetic exchange coupling through the 3d, 4d, and Sd transition metals. *Phys. Rev. Lett.* **1991**, *67*, 3598–3601. [CrossRef]
31. Grolier, V.; Renard, D.; Bartenlian, B.; Beauvillain, P.; Chappert, C.; Dupas, C.; Ferre, J.; Galtier, M.; Kolb, E.; Mulloy, M.; et al. Unambiguous evidence of oscillatory magnetic coupling between Co layers in ultrahigh vacuum grown Co/Au(111)/Co trilayers. *Phys. Rev. Lett.* **1993**, *71*, 3023–3026. [CrossRef] [PubMed]